Frequency-Domain Prony Method for Autoregressive Model Identification and Sinusoidal Parameter Estimation

Shigeru Ando, *Member, IEEE*

***Abstract*—In this study, the weighted integral method for identifying differential equation models is extended to a discrete-time system with a difference equation (DE) model and a finite-length sampled data sequence, and obtain a frequency-domain algorithm for short-time signal analysis and frequency estimation. The derivation consists of three steps. 1) Provide the DE (autoregressive model) with unknown coefficients, which is satisfied in a finite observation interval. 2) Discrete Fourier transform (DFT) the DE to obtain algebraic equations (AEs) among the Fourier coefficients. Two mathematical techniques are introduced to maintain the circulant nature of time shifts. 3) Simultaneously solve a sufficient number of AEs with least squares criterion to obtain unknowns exactly when the driving term is absent, or to obtain unknowns that minimize the driving power when it is present. The methods developed enable a decomposed processing of identification and estimation in the frequency domain. Thus, they will be suitable for maximizing statistical efficiency (smallness of estimation error variance), reducing the computational cost, and use in a resolution-enhanced time-frequency analysis of real-world signals. The performance of the proposed methods are compared with those of several DFT-based methods and Cramer–Rao lower bound. Also, the interference effect and its reduction in frequency-decomposed processing are examined.**

***Index Terms*—Prony method, autoregressive model, sinusoidal parameter estimation, weighted integral method, FFT.**

I. Introduction

THE Prony method [1], [2] is a procedure proposed more than two hundred years ago for determining the parameters of multiple damped sinusoids via the identification of an autoregressive (AR) model satisfied by their samples, and algebraic solutions of the characteristic equation. As a short-time exact direct method, it outperforms Fourier analysis in resolution and accuracy of signal modeling and parameter estimation. However, the Prony method behaves poorly against noise; the error keeps far away from the Cramer–Rao lower bound (CRLB). To overcome the ill conditions of the Prony method, a number of techniques have been proposed, including iterative filtering [3], [4], truncated singular value decomposition [5], [6], and the subspace-based methods [7], [8]. The subject has also been studied in the modern framework of compressed sensing and low-rank approximation [9], [10]. Several attempts have been made to find a closed-form formula that approximates the sinusoidal frequency using the discrete Fourier transform (DFT) results [11]–[13].

The problem of identifying and estimating signal models and parameters has been extensively studied and described in the literature [14]–[16]. It also has a wide range of emerging applications, including communications [17], power delivery [18], radar/sonar signal processing [19], instrumentation [20], and autonomous driving [21]. The data can either be real- or complex-valued, the model can either be stochastic or deterministic, and the sinusoids can either be single, ordered harmonics, or a random mixture. Our goal is to realize practical and superior performances in the analysis of real-world, real-valued signals with a rich deterministic nature such as music and speech, without any loss of the exactness and directness of the Prony method.

In recent years, we have developed the weighted integral method (WIM) for model parameter identification based on a differential equation formulation and finite duration observation [22]–[25]. A method for sinusoidal frequency estimate [22] has been shown to provide a statistical efficiency (smallness of estimation error variance) very close to CRLB. In this study, the principle is extended to a discrete-time system with difference equation (DE) modeling and finite-length sampled data sequence, and obtain a novel theory and algorithm for short-time signal analysis and spectral estimation. The performance is confirmed by comparing our method with other methods and CRLB. Also, the interference effect and its reduction in frequency-decomposed processing are examined.

II. Frequency-Domain Prony Method

A. Autoregressive (AR) Model

The AR model of order k is expressed as

$$f[t] = a_1 f[t-1] + a_2 f[t-2] + \cdots + a_k f[t-k] + \xi[t], \tag{1}$$

where t (integer) is the sample time, and $f[t]$ and $\xi[t]$ respectively are the signal and driving terms at t.

Given a finite sequence $f[t] (0 \le t \le N-1, N \gg k)$ satisfying this model as observation data, the coefficients $a_1, a_2, \ldots, a_k$ are estimated. This is the AR model identification. Frequencies

Manuscript received January 3, 2020; revised May 1, 2020; accepted May 26, 2020. Date of publication June 1, 2020; date of current version June 16, 2020. The associate editor coordinating the review of this manuscript and approving it for publication was Hsiao-Chun Wu.

The author is with the Professor Emeritus, University of Tokyo, Tokyo 113-8656, Japan (e-mail: Shigeru_Ando@ipc.i.u-tokyo.ac.jp).

Digital Object Identifier 10.1109/TSP.2020.2998929

and damping coefficients are obtained as algebraic solutions of the characteristic equation of DE. This is the sinusoidal parameter estimation based on the AR model.

B. Time-Domain Least Squares Identification

Typical methods for the AR model identification are in the time domain. The driving term $\xi[t]$ is assumed to be zero or sufficiently small in the observation interval $[0, N-1]$. Then, the simultaneous equation of (1) substituting the observed data is expressed as

$$\begin{bmatrix} f[k-1] & f[k-2] & \cdots & f[0] \\ f[k] & f[k-1] & \cdots & f[1] \\ \vdots & \vdots & & \vdots \\ f[N-2] & f[N-3] & \cdots & f[N-1-k] \end{bmatrix} \begin{bmatrix} a_1 \\ a_2 \\ \vdots \\ a_k \end{bmatrix} \simeq \begin{bmatrix} f[k] \\ f[k+1] \\ \vdots \\ f[N-1] \end{bmatrix}, \tag{2}$$

which can be solved by the least squares method. When the driving term is zero and the observation is free of noise, the above equation provides an exact solution of $a_1, \ldots, a_k$. This is the AR model identification in the Prony method. Since the data length N is finite, the left-hand-side matrix in the normal equation is not Toeplitz, in contrast with the Yule–Walker equation for the stationary stochastic process [15].

C. Frequency-Domain AR Model

From here, we describe how to convert the identification problem into the frequency domain, and obtain two methods inheriting the exactness and directness of the Prony method.

Assuming that Eq. (1) is satisfied in the observation interval, we apply a discrete version of mathematical techniques of WIM to this DE. Let the Fourier bases in the interval $[0, N-1]$ be $\{\Omega^{nt}\}(\Omega \equiv e^{-2\pi j/N}, n = 0, 1, \ldots, N-1, j$: imaginary unit). Then, the time-domain equalities are transformed identically to the frequency domain as

$$\begin{aligned} f[t] - \sum_{i=1}^{k} a_i f[t-i] = \xi[t] \quad {}^{\forall}t \in [0, N-1] \\ \longleftrightarrow \sum_{t=0}^{N-1} \Omega^{nt} \{f[t] - \sum_{i=1}^{k} a_i f[t-i]\} = \sum_{t=0}^{N-1} \Omega^{nt} \xi[t] \\ {}^{\forall}n \in [0, N-1]. \end{aligned} \tag{3}$$

Thus, among $f[t]$ and Fourier coefficients g_n and η_n of $f[t]$ and $\xi[t]$, respectively, N-tuple equalities hold that

$$g_n - \sum_{t=0}^{N-1} \Omega^{nt} \sum_{i=1}^{k} a_i f[t-i] = \eta_n \quad {}^{\forall}n \in [0, N-1], \tag{4}$$

where

$$g_n \equiv \sum_{t=0}^{N-1} \Omega^{nt} f[t], \eta_n \equiv \sum_{t=0}^{N-1} \Omega^{nt} \xi[t]. \tag{5}$$

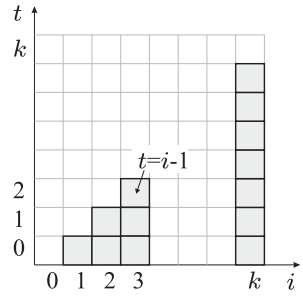

Fig. 1. Illustration of the interchange of summation of the contradictive component term of Eq. (8).

Unfortunately, however, the second term on the left-hand side of Eq. (4) involves signal samples $f[-1], \ldots, f[-k]$ outside the observation interval $[0, N-1]$; hence, it is not expressed by only the Fourier coefficients g_n and η_n observable to determine $a_i (i = 1, 2, \ldots, k)$.

D. Method 1: Circulantness via Extra Unknowns

To express the second term of Eq. (4) using g_n requires a circulant nature (circulantness, hereafter) of the shift operation in the observation interval. To incorporate this property, we rewrite the term as a sum of circulant (circularly shifting) terms and other extra terms as (see Fig. 1)

$$\begin{aligned} &\sum_{t=0}^{N-1} \Omega^{nt} \sum_{i=1}^{k} a_i f[t-i] \\ &= \sum_{i=1}^{k} a_i \sum_{t=0}^{N-1} \Omega^{nt} f[(t-i) \bmod N] - \sum_{i=1}^{k} a_i \sum_{t=0}^{i-1} \Omega^{nt} F_{t-i} \\ &= \sum_{i=1}^{k} a_i \Omega^{ni} \sum_{t=0}^{N-1} \Omega^{n(t-i)} f[(t-i) \bmod N] \\ &\quad - \sum_{t=0}^{k-1} \Omega^{nt} \sum_{i=t+1}^{k} a_i F_{t-i}, \end{aligned} \tag{6}$$

where

$$F_t \equiv f[t \bmod N] - f[t] (t = -k, -k+1, \ldots, -1) \tag{7}$$

are contradictive components for circulantness. By using the above, we express Eq. (4) as

$$g_n - \sum_{i=1}^{k} a_i \Omega^{ni} g_n - \sum_{i=0}^{k-1} \Omega^{ni} p_i = \eta_n, \tag{8}$$

where we define

$$p_i \equiv - \sum_{j=i+1}^{k} a_j F_{i-j} \qquad (i = 0, 1, \ldots, k-1) \tag{9}$$

as newly introduced unknowns including products of $F_t (t = -k, -k+1, \ldots, -1)$ and $a_i (i = 1, 2, \ldots, k)$. The minimization criterion of the driving term to determine unknowns from a

system of Eq. (8) for several different n is expressed as

$$(a_1, a_2, \ldots, a_k, p_0, p_1, \ldots, p_{k-1}) = \arg\min \sum_n \left| g_n - \sum_{i=1}^{k} a_i \Omega^{ni} g_n - \sum_{i=0}^{k-1} \Omega^{ni} p_i \right|^2, \quad (10)$$

where $\sum_n$ indicates a summation of all n used in the criterion. Since Eq. (8) is complex, a number of different $n (n > 0)$ larger than or equal to k is necessary. When the driving term is absent, this criterion provides the least squares solution (not in the rigorous sense, see the next paragraph), and provides an exact solution if observation noise is also absent. Therefore, by applying Eq. (10) regardless of the knowledge of the driving term, we can always expect a desirable solution in practical sense: the least squares solution when the driving term is absent and a minimizing solution of the driving term plus noise when the driving term is present. The residual sum after these optimization corresponds roughly to the squared sum of noise involved in g_n and/or the driving term.

Eq. (10) has the form of linear least squares problem with a direct (non-iterative) solution. It does not, however, imply the solution provides the least squares estimate or the minimum variance estimate. This is because the coefficients of unknowns $a_i (i = 1, 2, \ldots, k)$ are observed quantities involving noise. Since theoretical treatment is hard, we evaluate the goodness of estimate by numerical simulation (see Sections IV-A and IV-B). To achieve the maximum likelihood estimate of sinusoidal parameters, iterative procedure for nonlinear optimization is required [26]. The direct algebraic solution of these parameters obtainable without iteration via Eq. (10) and the characteristic algebraic equation will provide a good initial estimate for the iteration.

E. Method 2: Circulantness via Windowing of Equations

Let us rewrite the system of AR model equations in the interval $[0, N-1]$ as

$$\begin{bmatrix} f[0] & f[-1] & \cdots & f[-k] \\ f[1] & f[0] & \cdots & f[1-k] \\ \vdots & \vdots & & \vdots \\ f[N-1] & f[N-2] & \cdots & f[N-1-k] \end{bmatrix} \begin{bmatrix} -1 \\ a_1 \\ \vdots \\ a_k \end{bmatrix} = -\begin{bmatrix} \xi[0] \\ \xi[1] \\ \vdots \\ \xi[N-1] \end{bmatrix}, \quad (11)$$

and express the left-hand-side $N \times (k+1)$ matrix as a sum of the circulant $N \times (k+1)$ matrix and other $N \times k$ matrix (the first all-zero column is omitted) as

$$\begin{bmatrix} f[0] & f[N-1] & \cdots & f[N-k] \\ f[1] & f[0] & \cdots & f[N+1-k] \\ \vdots & \vdots & & \vdots \\ f[N-1] & f[N-2] & \cdots & f[N-1-k] \end{bmatrix} \begin{bmatrix} -1 \\ a_1 \\ \vdots \\ a_k \end{bmatrix} - \begin{bmatrix} f[N-1]-f[-1] & \cdots & f[N-k]-f[-k] \\ 0 & \cdots & f[N+1-k]-f[1-k] \\ \vdots & & \vdots \\ 0 & \cdots & 0 \end{bmatrix} \begin{bmatrix} a_1 \\ \vdots \\ a_k \end{bmatrix} = -\begin{bmatrix} \xi[0] \\ \xi[1] \\ \vdots \\ \xi[N-1] \end{bmatrix}. \quad (12)$$

The $N \times k$ matrix in the second line is nonzero only from its first to kth rows. Therefore, by multiplying from the left an $N \times N$ diagonal matrix

$$\boldsymbol{W} = \mathrm{diag}(0, \ldots, 0, w_k, \ldots, w_{N-1}) \quad (13)$$

whose elements from (1, 1) to (k, k), i.e., $w_0, w_1, \ldots, w_{k-1}$, are zero, eliminates all the nonzero terms of the $N \times k$ matrix, and results in the equation

$$\boldsymbol{W} \begin{bmatrix} f[0] & f[N-1] & \cdots & f[N-k] \\ f[1] & [(0] & \cdots & f[N+1-k] \\ \vdots & \vdots & & \vdots \\ f[N-1] & f[N-2] & \cdots & f[N-1-k] \end{bmatrix} \begin{bmatrix} -1 \\ a_1 \\ \vdots \\ a_k \end{bmatrix} = -\boldsymbol{W} \begin{bmatrix} \xi[0] \\ \xi[1] \\ \vdots \\ \xi[N-1] \end{bmatrix}, \quad (14)$$

in which noncirculant terms are all removed (windowing operation of AR model equations). Actually, the above equation is equivalent to a system of AR equations expressed only by samples in $[0, N-1]$. Newly introduced parameters $w_k, w_{k+1}, \ldots, w_{N-1}$ are the weights for each equation. A method to determine them is shown in the next section.

Here, we introduce the Fourier transform matrix

$$\boldsymbol{\mathcal{F}} \equiv \left[\Omega^{(i-1)(j-1)}\right], \Omega \equiv e^{-2\pi j/N}, \quad (15)$$

where i, j in the exponent of $\Omega^{(i-1)(j-1)}$ are the column and row orders of $\boldsymbol{\mathcal{F}}$. Since $\boldsymbol{\mathcal{F}}/\sqrt{N}$ is unitary, it follows that

$$\boldsymbol{\mathcal{F}}^{-1}\boldsymbol{\mathcal{F}} = I, \quad \boldsymbol{\mathcal{F}}^{*}\boldsymbol{\mathcal{F}} = NI, \quad \boldsymbol{\mathcal{F}}^{-1} = \frac{1}{N}\boldsymbol{\mathcal{F}}^{*}. \quad (16)$$

Therefore, by multiplying $\boldsymbol{\mathcal{F}}$ from the left, and replacing $\boldsymbol{W}$ with $\boldsymbol{W}\boldsymbol{\mathcal{F}}^{-1}\boldsymbol{\mathcal{F}}$, we obtain

$$\boldsymbol{\mathcal{F}}\boldsymbol{W}\boldsymbol{\mathcal{F}}^{-1}\boldsymbol{\mathcal{F}}\begin{bmatrix} f[0] & f[N-1] & \cdots & f[N-k] \\ f[1] & f[0] & \cdots & f[N+1-k] \\ \vdots & \vdots & & \vdots \\ f[N-1] & f[N-2] & \cdots & f[N-1-k] \end{bmatrix}\begin{bmatrix} -1 \\ a_1 \\ \vdots \\ a_k \end{bmatrix}$$
$$= -\boldsymbol{\mathcal{F}}\boldsymbol{W}\boldsymbol{\mathcal{F}}^{-1}\boldsymbol{\mathcal{F}}\begin{bmatrix} \xi[0] \\ \xi[1] \\ \vdots \\ \xi[N-1] \end{bmatrix}, \tag{17}$$

Hence, denoting $\boldsymbol{Q} \equiv \boldsymbol{\mathcal{F}}\boldsymbol{W}\boldsymbol{\mathcal{F}}^{-1}$, we obtained

$$\boldsymbol{Q}\begin{bmatrix} g_0 & g_0 & \cdots & g_0 \\ g_1 & \Omega g_1 & \cdots & \Omega^k g_1 \\ \vdots & \vdots & & \vdots \\ g_{N-1} & \Omega^{N-1} g_{N-1} & \cdots & \Omega^{(N-1)k} g_{N-1} \end{bmatrix}\begin{bmatrix} -1 \\ a_1 \\ \vdots \\ a_k \end{bmatrix}$$
$$= -\boldsymbol{Q}\begin{bmatrix} \eta_0 \\ \eta_1 \\ \vdots \\ \eta_{N-1} \end{bmatrix}, \tag{18}$$

in which only the Fourier coefficients g_n and η_n of $f[t]$ and $\xi[t]$, respectively, in the interval $[0, N-1]$ are involved. The matrix $\boldsymbol{Q}$ in Eq. (18) has the form

$$\boldsymbol{Q} = \boldsymbol{\mathcal{F}}\text{diag}(0, \ldots, 0, w_k, \ldots, w_{N-1})\boldsymbol{\mathcal{F}}^{-1}$$
$$= \frac{1}{N}\begin{bmatrix} \sum w_t & \sum w_t\Omega^{-t} & \cdots & \sum w_t\Omega^{-t(N-1)} \\ \sum w_t\Omega^{t} & \sum w_t & \cdots & \sum w_t\Omega^{-t(N-2)} \\ \vdots & \vdots & & \vdots \\ \sum w_t\Omega^{t(N-1)} & \sum w_t\Omega^{t(N-2)} & \cdots & \sum w_t \end{bmatrix} \tag{19}$$

and is an $N \times N$ circulant matrix with rank $N-k$ whose (i,j) element is expressed as

$$q_{ij} = \frac{1}{N}\sum_{t=k}^{N-1} w_t\Omega^{(i-j)t} \equiv \tilde{q}_{i-j}. \tag{20}$$

To simplify further, we express the Fourier coefficients after a circular convolution by $\boldsymbol{Q}$ as

$$\begin{bmatrix} \tilde{q}_0 & \tilde{q}_{-1} & \cdots & \tilde{q}_1 \\ \tilde{q}_1 & \tilde{q}_0 & \cdots & \tilde{q}_2 \\ \vdots & \vdots & & \vdots \\ \tilde{q}_{N-1} & \tilde{q}_{N-2} & \cdots & \tilde{q}_0 \end{bmatrix}\begin{bmatrix} g_0 \\ \Omega^i g_1 \\ \vdots \\ \Omega^{i(N-1)} g_{N-1} \end{bmatrix}$$
$$\equiv \begin{bmatrix} g_0^{[i]} \\ g_1^{[i]} \\ \vdots \\ g_{N-1}^{[i]} \end{bmatrix}, \tag{21}$$

($\tilde{q}_{-1} = \tilde{q}_{N-1}$), or equivalently as

$$g_n^{[m]} = \sum_{j=0}^{N-1} q_{n+1,j+1}\Omega^{jm} g_j = \sum_{j=-N/2}^{N/2-1} \tilde{q}_{-j}\Omega^{(n+j)m} g_{n+j}, \tag{22}$$

where in $g_n^{[m]}$, the subscript n is the frequency and the superscript m is the delay time. Then, Eq. (18) is rewritten as the system of frequency-wise AR equations:

$$\begin{bmatrix} g_0^{[0]} \\ g_1^{[0]} \\ \vdots \\ g_{N-1}^{[0]} \end{bmatrix} = \begin{bmatrix} g_0^{[1]} & g_0^{[2]} & \cdots & g_0^{[k]} \\ g_1^{[1]} & g_1^{[2]} & \cdots & g_1^{[k]} \\ \vdots & \vdots & & \vdots \\ g_{N-1}^{[1]} & g_{N-1}^{[2]} & \cdots & g_{N-1}^{[k]} \end{bmatrix}\begin{bmatrix} a_1 \\ a_2 \\ \vdots \\ a_k \end{bmatrix} + \begin{bmatrix} \eta_0^{[0]} \\ \eta_1^{[0]} \\ \vdots \\ \eta_{N-1}^{[0]} \end{bmatrix}. \tag{23}$$

The criterion for the least squares solution when the driving term is absent or for the minimization of an unknown driving term is expressed as

$$(a_1, a_2, \ldots, a_k) = \arg\min \sum_n \left| g_n^{[0]} - \sum_{i=1}^{k} a_i g_n^{[i]} \right|^2, \tag{24}$$

where $\sum_n$ is a summation of all n in the minimization. To construct criterion (24), no negative frequency is necessary because for real signals,

$$g_{N-n}^{[m]} = (g_n^{[m]})^* \tag{25}$$

Thus, they do not provide independent equations.

Note that the window sequence $(0, \ldots, 0, w_k, \ldots, w_{N-1})$ introduced above differs from the conventional window function multiplied directly with data. Windowing of data corrupts their fitness to the AR model. In contrast, the windowing of equations does not affect the consistency between them; thus, the exactness of the Prony method is still maintained.

F. Design of Window Sequence $w_k, w_{k+1}, \ldots, w_{N-1}$

In Eq. (18), multiplication of $\boldsymbol{Q}$ and the $N \times (k+1)$ matrix is a convolution of the Fourier coefficients. Therefore, quite similarly to conventional window functions, choosing $\boldsymbol{Q}$ having a minimum extent of convolution will reduce the mixing among frequency components. This is advantageous for selectivity and isolation in the frequency domain of $g_n^{[m]}, \eta_n^{[m]} (0 \leq m \leq k)$, and an equation expressed by each row of Eq. (23). This condition is satisfied when we construct the sequence $0, \ldots, 0, w_k, w_{k+1}, \ldots, w_{N-1}$ with a minimum number of lowest-frequency Fourier bases.

When the order is k (multiple of 2), the weight sequence with the minimum extent being symmetric in its nonzero interval is

expressed as

$$w_t = \sum_{i=0}^{k/2} c_i \cos\left(i\left(t - \frac{k-1}{2}\right)\Delta_\omega\right), \tag{26}$$

hence, the elimination conditions of non-circulant terms are

$$w_0 = w_{k-1} = \sum_{i=0}^{k/2} c_i \cos\left(i\left(\frac{k-1}{2}\right)\Delta_\omega\right) = 0, \tag{27}$$

$$w_1 = w_{k-2} = \sum_{i=0}^{k/2} c_i \cos\left(i\left(\frac{3k-1}{2}\right)\Delta_\omega\right) = 0, \tag{28}$$

$$\vdots$$

$$w_{k/2-1} = w_{k/2} = \sum_{i=0}^{k/2} c_i \cos\left(i\frac{\Delta_\omega}{2}\right) = 0. \tag{29}$$

Simultaneously solving these equations and a normalization, e.g., $c_0 = 1$, uniquely provides the coefficients $c_0, c_1, \ldots, c_{k/2}$. From these coefficients, the circulant elements of $\boldsymbol{Q}$ are obtained as

$$\tilde{q}_j = \begin{cases} c_0 = 1 & (j = 0) \\ \frac{1}{2}c_j \Omega^{j(k-1)/2} & (0 < j \le k/2) \\ \frac{1}{2}c_{-j} \Omega^{j(k-1)/2} & (-k/2 \le j < 0) \\ 0 & (\text{otherwise}) \end{cases}. \tag{30}$$

Fig. 2 shows an example of frequency and time distributions of the window sequence when $N = 64$ and $k = 8$.

For designing the window sequence, the use of k larger than the required value (double the number of sinusoids to be simultaneously estimated) is possible. In this case, the zero portion of the sequence is extended and the rising and falling edges from it becomes smoother (the higher-order difference becomes zero). This is useful for enhancing the interference reduction capability between proximate sinusoids (see Section IV-C).

III. Parallel Array of Single-Tone Estimators

As shown in Eqs. (8) and (23), the frequency domain Prony method works nearly frequency-wise. This means that a mixture of sinusoidal components in the observed signal can be separated and aggregated into different peaks during the frequency analysis for the calculation of g_n or $g_n^{[m]}$. Therefore, unlike a total estimate of all sinusoids in the Prony method, a practical approach of component-wise estimation is possible, in which an isolated sinusoid is determined using a minimum number of Fourier coefficients involving the component. Around the peak, the sinusoidal parameters are estimated with the best signal-to-noise ratio (SNR) and isolation from other sinusoids. Even between peaks, parameters of a proximate sinusoid contributing most to the Fourier coefficients can be estimated. This component-wise approach also solves the order estimation problem in the Prony method and greatly reduces the computational cost of a high-order algebraic equation.

Another benefit of this approach is the geometrical freedom to construct the time-frequency space. By making the procedure as an estimation unit that is independent and localized both in time and frequency, we can carry out the parallel and variable construction of time-frequency space. To discriminate proximate sinusoids, if found, we can apply a multi-tone estimation method (combination of Eqs. (8) or (23)) there.

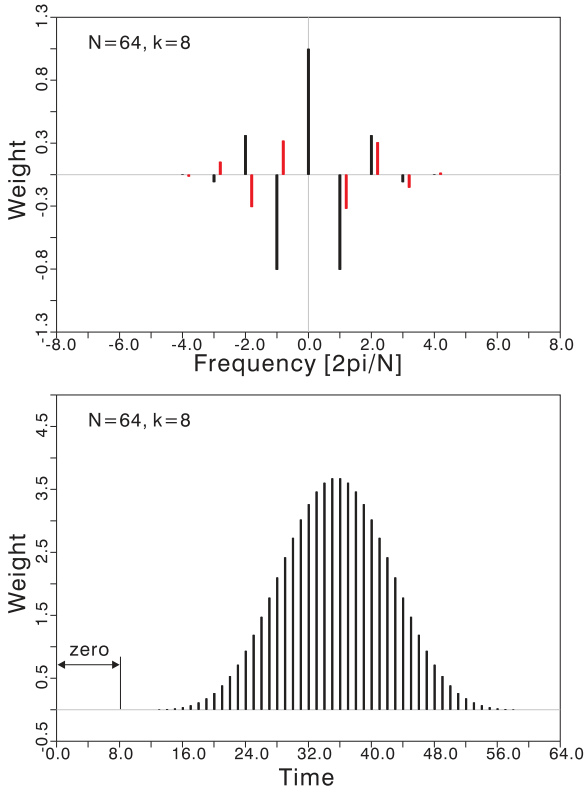

Fig. 2. An example of window sequence in time domain (bottom) and circulant convolution sequence in frequency domain (top) of the windowing-of-equation method ($k = 8, N = 64$). Black bar: real part, red bar: imaginary part.

A. Equations for Single Sinusoid

The target is a single damped sinusoid

$$f[t] = Ae^{-\zeta t}\cos(\omega t + \phi), \tag{31}$$

where ω, ζ, A, and ϕ are the frequency, damping coefficient, amplitude, and phase, respectively. The sinusoid is the general solution of

$$f[t] - (2e^{-\zeta}\cos\omega)f[t-1] + e^{-2\zeta}f[t-2] = 0, \tag{32}$$

which is the case when $k = 2, a_1 = 2e^{-\zeta}\cos\omega, a_2 = -e^{-2\zeta}$, and $\xi[t]$ is absent in Eq. (1). Therefore, Eq. (8) for Method 1 using extra unknowns for circulantness is expressed as

$$\left[\Omega^n g_n \ \Omega^{2n} g_n \ 1 \ \Omega^n\right]\left[a_1 \ a_2 \ p_0 \ p_1\right]^t = g_n. \tag{33}$$

It has four real unknowns and the equality is complex providing two real constraints. Therefore, two or more equations with different n are required to determine the unknowns. In the case of Method 2 based on the windowing of equations, the unknowns a_1 and a_2 are obtained by solving

$$\begin{bmatrix} g_n^{[1]} & g_n^{[2]} \end{bmatrix}\begin{bmatrix} a_1 \\ a_2 \end{bmatrix} = g_n^{[0]}, \tag{34}$$

where

$$g_n^{[m]} = \tilde{q}_1 \Omega^{(n-1)m} g_{n-1} + \tilde{q}_0 \Omega^{nm} g_n + \tilde{q}_{-1} \Omega^{(n+1)m} g_{n+1},$$
$$\tilde{q}_1 = -\frac{1}{2}\left(1 - j\tan\left(\frac{\Delta_\omega}{2}\right)\right), \tilde{q}_0 = 1,$$
$$\tilde{q}_{-1} = -\frac{1}{2}\left(1 + j\tan\left(\frac{\Delta_\omega}{2}\right)\right), \quad (35)$$

which provides two real constraints for two real unknowns. Therefore, a single n is sufficient to determine ω and ζ. Note that three Fourier coefficients g_{n-1}, g_n, and g_{n+1} are required to calculate $g_n^{[0]}, g_n^{[1]}$, and $g_n^{[2]}$.

B. Three Fourier Coefficients Real-Constrained (3F-R) Method

In order to obtain Method 1 for the single-tone estimate, the use of three adjacent frequencies, $n-1, n$, and $n+1$, is a natural choice. This provides the same condition of inputs, g_{n-1}, g_n, and g_{n+1} as the windowing method (Method 2). The simultaneous equation is written as

$$\begin{bmatrix} \Omega^{n-1} g_{n-1} & \Omega^{2(n-1)} g_{n-1} & 1 & \Omega^{n-1} \\ \Omega^n g_n & \Omega^{2n} g_n & 1 & \Omega^n \\ \Omega^{n+1} g_{n+1} & \Omega^{2(n+1)} g_{n+1} & 1 & \Omega^{n+1} \end{bmatrix} \begin{bmatrix} a_1 \\ a_2 \\ p_0 \\ p_1 \end{bmatrix} \simeq \begin{bmatrix} g_{n-1} \\ g_n \\ g_{n+1} \end{bmatrix}, \quad (36)$$

which is solved in the least squares sense constraining all the solutions to be real. The FFT is used to fast obtain the Fourier coefficients g_{n-1}, g_n, and g_{n+1} from observation data for all n. The damping coefficient and frequency are obtained using the relations $a_1 = 2e^{-\zeta}\cos\omega$ and $a_2 = -e^{-2\zeta}$ as

$$\zeta = -\frac{1}{2}\log(-a_2), \quad \omega = \cos^{-1}\left(\frac{a_1}{2\sqrt{-a_2}}\right). \quad (37)$$

After ζ and ω are determined, the amplitude and phase of the sinusoid are estimated by a linear least squares fitting of corresponding Fourier coefficients [22].

To obtain reliability measures, express Eq. (36) as $\boldsymbol{A}\boldsymbol{x} = \boldsymbol{b}$. Then, the residual error of the least squares estimate is

$$J_{RES} \equiv \boldsymbol{b}^\dagger \boldsymbol{b} - (\boldsymbol{A}^\dagger \boldsymbol{b})^\dagger \boldsymbol{x}, \quad (38)$$

where $\dagger$ denotes the conjugate transpose. J_{RES} becomes large when the fitness of the AR model without driving becomes worse; e.g., mixture condition of two or more sinusoids or the presence of the driving term in the observation interval. For judging these conditions, the estimation error covariance matrix can be predicted from J_{RES} as

$$\boldsymbol{J}_{ERR} = \frac{J_{RES}}{3}(\boldsymbol{A}^\dagger \boldsymbol{A})^{-1}, \quad (39)$$

which provides a measure of unreliability of the estimate. Assuming $\zeta \simeq 0$, and thus $a_2 \simeq -1$, the estimation errror variance σ_ω^2 of ω is obtained as

$$\frac{\partial \omega}{\partial a_1} = -\frac{1}{2\sqrt{1 - a_1^2/4}} \text{ thus } \sigma_\omega^2 = \frac{1}{4 - a_1^2}\sigma_{a1}^2, \quad (40)$$

where σ_{a1}^2 is a (1, 1) element of $\boldsymbol{J}_{ERR}$.

C. Double Tone Extention of 3F-R Method

For use in experimental comparison, we define here the six Fourier coefficients, two sinusoidal frequency, real-constrained (6F2-R) method. Let n and $m > n$ be the orders of the Fourier coefficient at two proximate peaks. If $m - n \leq 2$, they are increased or decreased so that the six Fourier coefficients have no overlaps. Then, the system of equations is expressed as

$$\begin{bmatrix} \Omega^{n-1} g_{n-1} & \cdots & \Omega^{4(n-1)} g_{n-1} & 1 & \cdots & \Omega^{3(n-1)} \\ \Omega^n g_n & \cdots & \Omega^{4n} g_n & 1 & \cdots & \Omega^{3n} \\ \Omega^{n+1} g_{n+1} & \cdots & \Omega^{4(n+1)} g_{n+1} & 1 & \cdots & \Omega^{3(n+1)} \\ \Omega^{m-1} g_{m-1} & \cdots & \Omega^{4(m-1)} g_{m-1} & 1 & \cdots & \Omega^{3(m-1)} \\ \Omega^m g_m & \cdots & \Omega^{4m} g_m & 1 & \cdots & \Omega^{3m} \\ \Omega^{m+1} g_{m+1} & \cdots & \Omega^{4(m+1)} g_{m+1} & 1 & \cdots & \Omega^{3(m+1)} \end{bmatrix} \times \begin{bmatrix} a_1 \\ \vdots \\ a_4 \\ p_0 \\ \vdots \\ p_3 \end{bmatrix} \simeq \begin{bmatrix} g_{n-1} \\ g_n \\ g_{n+1} \\ g_{m-1} \\ g_m \\ g_{m+1} \end{bmatrix}, \quad (41)$$

which is solved by the least squares method. Two sinusoidal parameters (ζ_1, ω_1) and (ζ_2, ω_2) are obtained from the roots $\alpha_1, \alpha_1^*, \alpha_2$, and α_2^* of the characteristic algebraic equation

$$a_4 z^4 + a_3 z^3 + a_2 z^2 + a_1 z - 1 = 0, \quad (42)$$

where $\alpha_1 = e^{-\zeta_1 + j\omega_1}$ and $\alpha_2 = e^{-\zeta_2 + j\omega_2}$.

D. Three Fourier Coefficients Windowing (3F-W) Method

As Method 2 for the single-tone estimate with windowing of equations, the unique solution of Eq. (34) is obtained as follows:

$$a_1 = \frac{\Im g_n^{[2]} \Re g_n^{[0]} - \Re g_n^{[2]} \Im g_n^{[0]}}{\Re g_n^{[1]} \Im g_n^{[2]} - \Re g_n^{[2]} \Im g_n^{[1]}}, \quad (43)$$
$$a_2 = \frac{\Re g_n^{[1]} \Im g_n^{[0]} - \Im g_n^{[1]} \Re g_n^{[0]}}{\Re g_n^{[1]} \Im g_n^{[2]} - \Re g_n^{[2]} \Im g_n^{[1]}}, \quad (44)$$

where $\Re$ and $\Im$ indicate the real part and imaginary part, respectively. The conversion from a_1, a_2 to ζ, ω and the estimation of the amplitude and phase of the sinusoid are the same as those in the 3F-R method.

E. Condition for Unique Solution

To simplify the problem, we assume $\zeta = 0$ or ζ is known. Then, the determinant of the left-hand-side matrix to obtain

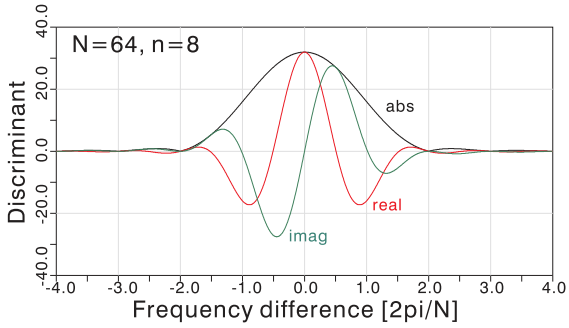

Fig. 3. A graph of frequency-difference dependence of the discriminant D $(N = 64, n = 8)$ between the target frequency of sinusoid and the center frequency of the estimator.

TABLE I
COMPARISON OF COMPUTATION OPERATIONS AMONG THE PROPOSED METHODS AND TYPICAL DFT-BASED METHODS. EACH CELL INDICATES NUMBERS OF: MULTIPLY (DIVIDE, MATH-FUNCTION) IN TYPICAL IMPLEMENTATION. OPERATIONS FOR FFT ARE NOT INCLUDED

method	convolution in frequency domain	estimation equation	mathematical function used
3F-R	–	53 (2,1)	$\cos^{-1}$
3F-W	24(0,0)	28 (1,1)	$\cos^{-1}$
Quinn[11]	–	7 (4,0)	–
Macleod[12]*	–	10 (2,1)	sqrt
Candan[13]	–	7 (1,0)	–

(*"nearly optimal three-sample interpolator" method).

a_1, p_0, p_1 has the form

$$\det\begin{bmatrix} \Omega^{n-1}g_{n-1} & \Omega^{n-1} & 1 \\ \Omega^{n}g_{n} & \Omega^{n} & 1 \\ \Omega^{n+1}g_{n+1} & \Omega^{n+1} & 1 \end{bmatrix}$$
$$= \Omega^{2n-1/2}(\Omega-1)\left(-\Omega^{-1/2}g_{n-1} + (\Omega^{1/2}+\Omega^{-1/2})g_n - \Omega^{1/2}g_{n+1}\right). \quad (45)$$

Therefore, the condition is expressed as

$$D \equiv -\Omega^{-1/2}g_{n-1} + \left(\Omega^{1/2}+\Omega^{-1/2}\right)g_n - \Omega^{1/2}g_{n+1}$$
$$= 2\sum_{t=0}^{N-1}\left(\cos\left(\frac{\Delta_\omega}{2}\right) - \cos\left(\Delta_\omega\left(t+\frac{1}{2}\right)\right)\right)f[t]\Omega^{nt}$$
$$\neq 0, \quad (46)$$

whichis in proportion to the Fourier coefficient of the observed signal multiplied by a weight distribution similar to the Hann window function expressed as

$$\cos\left(\frac{\Delta_\omega}{2}\right) - \cos\left(\Delta_\omega\left(t+\frac{1}{2}\right)\right) \quad (0 \le t \le N-1). \quad (47)$$

Fig. 3 shows plots of the frequency-difference dependence of D for a unit-amplitude sinusoid

$$f[t] = \cos((n+\delta)\Delta_\omega t), \quad (48)$$

whereδ is the normalized frequency difference from the central frequency order n of the estimator. Since D is zero at integer δ except for $-1, 0, 1$, and is nonzero between them, D remains nonzero for $-2\Delta_\omega < \delta < 2\Delta_\omega$. This means that if we choose n such that either $n-1, n$, or $n+1$ is at the peak of the Fourier coefficient distribution, the estimator can provide a unique solution. Of course, it is not always the case if significant noise is present. Since

$$g_n^{[1]} = \frac{\Omega^n}{2\cos(\Delta_\omega/2)}D, \quad (49)$$

the above uniqueness condition also applies to the 3F-W method to estimate a_1 assuming a zero or known ζ.

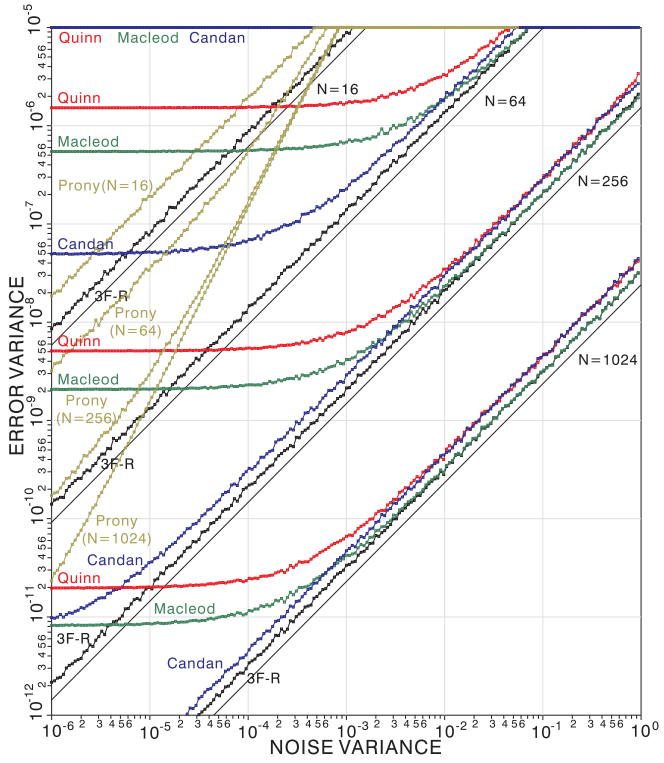

Fig. 4. Comparison of proposed method 3F-R (black) with Quinn's (red), Macleod's (green), Candan's (blue), and Prony (dark yellow) methods. Approximation methods (Quinn's, Macleod's, Candan's) show saturation of accuracy (no decrease in estimation error variance) under high-SNR conditions. The proposed method (3F-R) does not show saturation and is close to CRLB in all conditions.

IV. NUMERICAL EVALUATION

A. Comparison with Other Methods and CRLB

Repetitive numerical simulation was performed using different waveforms with varying phase and added white noise variance. Fig. 4 shows graphs of the estimation error variance of frequency ω versus noise variance in various DFT-based methods for a single sinusoid. The observation interval N was from 16 to 1024, as indicated in the graph. For the target sinusoid $f[t] = \cos(\omega t + \phi) + \eta[t](0 \le t \le N-1)$ with noise $\eta[t]$, frequencies $\omega = (N/8 + i/4)\Delta_\omega (i = 0, 1, 2, 3)$, zero damping coefficient, and unit amplitude were assumed. For each condition, phase $\phi \in [0, 2\pi]$ was varied in $\pi/180$ steps and the results were averaged. The graphs of CRLB for amplitude A and noise

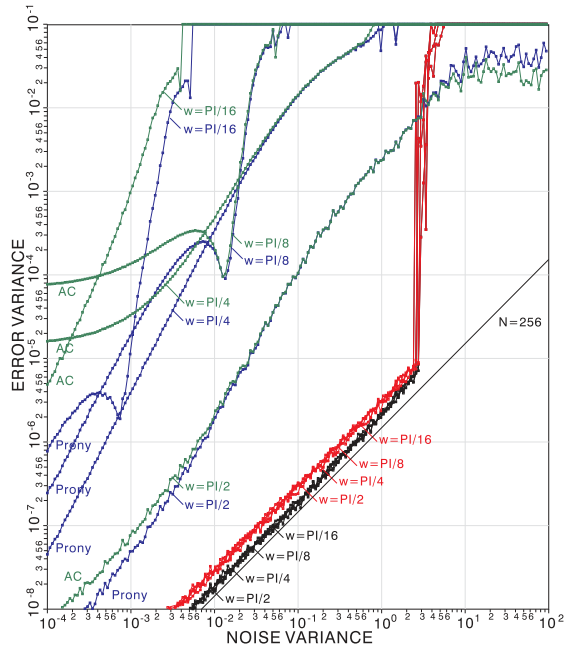

Fig. 5. Frequency dependence of accuracies of 3F-R, 3F-W, Prony, and autocorrelation (AC) methods under medium- to low-SNR conditions: 3F-R (black), 3F-W (red), Prony (blue), and AC (green) methods. $N = 256$, and frequency $\omega = \pi/2, \pi/4, \pi/8$, and $\pi/16$. In the Prony and AC methods, the deviations from CRLB become larger at low sinusoidal frequencies. In the proposed methods (3F-R and 3F-W), no frequency dependences are evident and the accuracies are always close to CRLB. Abrupt increases in error of the proposed methods are due to a false choice of noise peak for estimation.

variance σ^2 expressed as [27]

$$\text{CRLB} = \sqrt{24}(\sigma/A)(N^3 - N)^{-0.5} \tag{50}$$

are also shown as thin solid lines. The DFT interpolation methods, i.e., Quinn's [11], Macleod's [12], and Candan's [13] methods, provide estimation error variance comparable to CRLB under low SNR conditions. However, the reduction in error variance under high SNR conditions comes to an end, which is due to a systematic error (bias) involved in these methods. In the Prony method, no accuracy saturation takes place because of its exactness, but its error variance is far larger than CRLB particularly for large N. In contrast to these methods, the accuracy of the 3F-R method shows no saturation and approaches CRLB very closely in all conditions. As shown in Table I, computational operations for estimation are almost comparable to those of the DFT-based methods with an excellent computational efficiency. Note that the close proximity to CRLB at any data length and SNR assures an ideal accuracy regardless of the tradeoff between time and frequency resolutions.

B. Comparisons under Wide Frequency and Low-SNR Conditions

Fig. 5 shows the estimation error variances of the 3F-R, 3F-W, Prony, and autocorrelation (AC) methods for a single sinusoid with frequency $\omega = \pi/16, \pi/8, \pi/4$, and $\pi/2$ ($\pi = N\Delta_\omega/2$ is the Nyquist frequency) and $N = 256$. The range of noise variances was shifted from those in Fig. 4 to include low-SNR conditions. In the AC method, the left-hand side matrix of the Yule–Walker equation is calculated as Toeplitz. In the Prony and AC methods, the lower the frequency is, the larger the deviation from CRLB becomes. This is due to the use of a proximate set of data that are largely correlated. Deviations of the AC method are almost always larger than the Prony method. It will be because an additional step for constructing an autocorrelation function from finite data intoduces a bias. In contrast, the frequency-domain Prony, 3F-R, and 3F-W methods are free from the frequency-dependent deviation from CRLB. This is because they rely on the changes in Fourier coefficients that are mostly uncorrelated with each other. The deviations of the curves obtained by the 3F-W method (red lines) from CRLB are slightly larger than those obtained by the 3F-R method (black lines). This is due to a windowing loss of data and lack of real-value constraints on noncirculant terms in the 3F-W method.

Under low-SNR conditions (right side of Fig. 5), the 3F-R and 3F-W methods suffer an abrupt increase in error. This is due to a false peak of Fourier coefficients caused by larger power of noise than the sinusoid. In the Prony and AC methods, no such increases take place.

C. Comparison of Single- and Double-Tone Estimators under Mixture Condition

Fig. 6(a) shows the interference between proximate sinusoids when single-tone estimators (3F-R, 3F-W) are applied peak by peak in the Fourier coefficient distribution, and the result of the application of a double-tone estimator (6F2-R) around the two peaks. As the signal, two unit-amplitude sinusoids with the frequency range $[\pi/8, 3\pi/8]$ and frequency difference range $[-5\Delta_\omega, 5\Delta_\omega]$ are added to each other with 1% white Gaussian noise. The phase of the second sinusoid was uniformly varied in $[-\pi, \pi]$. When the frequency difference is smaller than about $3\Delta_\omega$, the interference, i.e., bias and phase dependence of estimated results, becomes significant in both the 3F-R and 3F-W methods. The estimates of damping coefficient ζ are also non zero in this range. Outside of $3\Delta_\omega$, the interference decreases very rapidly. The decrease observed in the 3F-W method seems to be faster than in the 3F-R method. In contrast, in the 6F2-R method, no interference is found for almost all frequency differences. When two frequencies are nearly identical, however, the results show a large bias and phase dependence. This is due to a disagreement between the given and actual numbers of sinusoids because two frequencies are degenerating into a single one.

Fig. 6(b) shows the spectral distribution of estimated sinusoids calculated as

$$|H(\omega)| = \left| \frac{A_1 e^{j\phi_1}}{e^{j\omega} - e^{-\zeta_1 + j\omega_1}} + \frac{A_2 e^{j\phi_2}}{e^{j\omega} - e^{-\zeta_2 + j\omega_2}} \right|,$$

where $\zeta_1, \omega_1, A_1, \phi_1$ and $\zeta_2, \omega_2, A_2, \phi_2$ are the damping coefficient, frequency, amplitude, and phase of the first and second sinusoids, respectively. To illustrate the estimated amplitude, the peak height of each sinusoid is clipped at the corresponding level. In the 6F2-R results, peaks of sinusoids are clearly separated except for the degenerating case. Further consideration will

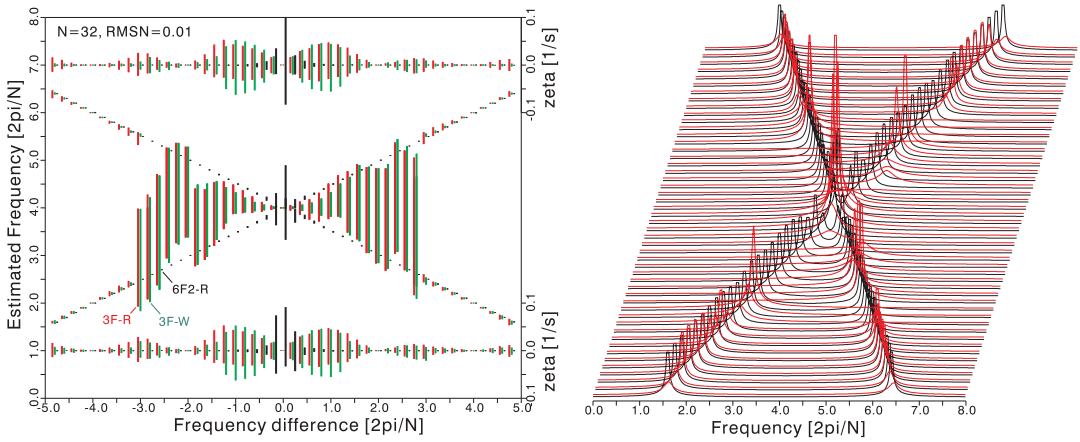

(a) sinusoidal parameters vs. frequency difference (b) spectral distribution plots of (a)

Fig. 6. Interference between proximate sinusoids with 3F-R and 3F-W methods, and its resolution with 6F2-R method ($N = 32$, 1% noise). (a) Distributions of estimated parameters. Vertical bars: error bars of results under various phase differences (3F-R: red, 3F-W: green, 6F2-R: black). Central graphs: estimated frequency ω (left axis scale). Top-side graphs: estimated damping coefficient ζ for upper-frequency sinusoid (top-right axis scale). Bottom-side graphs: estimated ζ for lower-frequency sinusoid (bottom-right axis scale). (b) Spectral distribution of estimated results of (a) (3F-R: red, 6F2-R: black). Peak heights indicate the estimated amplitudes of sinusoid.

be needed, however, regarding the use of spectral expressions in the Prony and proposed method, which are valid for finite duration data without a stationarity assumption.

D. Examination Using Musical and Speech Data

We show some experiments of examining practical performances towards future applications of the proposed method.

Figs. 7(a) and (b) show results of the short-time Fourier transform (STFT) and the single-tone estimator array (3F-W) to a musical sound (flute solo and orchestra). In both results, the vertical axis is log frequency and the horizontal axis is time. To observe the change in sound streams, $\sim$4 s is decimated into the range of the horizontal axis. For the 3F-W method, the results are plotted as dots at the estimated frequencies. The brightness and hue of a dot indicate the amplitude and unreliability measure, respectively, from blue (high reliability) to red (low reliability). With the interval $N = 2048$ and thus $T = 46.4$ ms, high-frequency harmonic sequences are captured well by both the STFT and 3F-W methods. In the low frequency range, however, peaks of STFT become unclear because of insufficient frequency resolution of Fourier bases for describing the harmonics of low-fundamental sounds. In contrast, the 3F-W method (b) shows significant improvements in capturing the harmonics as traces of condensed dots of estimated frequencies.

Figs. 7(c) and (d) show results for a male voice "a-i-u-e-o" ($\sim$1 s). In (c), by taking a shorter observation interval than the pitch interval ($N = 64, T = 4$ ms), we extract formant frequencies directly as the traces. Large scatter and large unreliability measures being synchronous to pitch are caused by the impulsive excitation sequence. In (c) for a longer observation interval ($N = 256, T = 16$ ms), traces of pitch and its harmonics are extracted in a modulated manner: the amplitudes of traces of

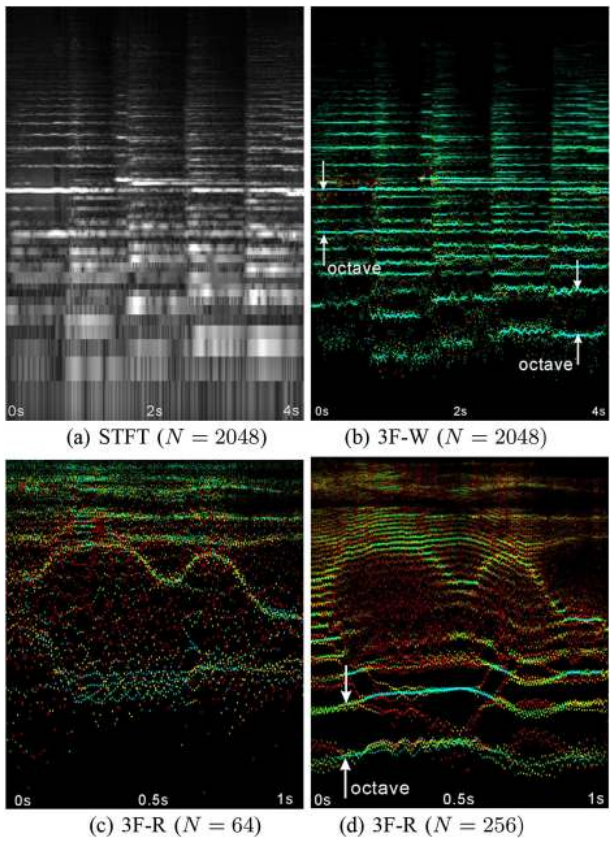

(a) STFT ($N = 2048$) (b) 3F-W ($N = 2048$)

(c) 3F-R ($N = 64$) (d) 3F-R ($N = 256$)

Fig. 7. Applications to musical and speech signals. (a), (b): Results of applying STFT and 3F-W methods at $\sim$4 s into the opening of J. S. Bach, BWV1067 no. 5. (central two traces are the 1st and 2nd harmonics of flute solo). The vertical and horizontal axes are log frequency and time (1/256 down-sampled from $f_s = 44.1$ kHz). The color indicates ζ^2 of the estimate (blue: small, red: large). (c), (d): Results for NII SRC [28] speech data "a-i-u-e-o" ($f_s = 16$ kHz, down-sampling rate of time axis is 1/32), the color indicates the unreliability measure σ_ω^2 of the estimate (blue:small, red:large). A bit scattered traces of formants in (c) and combined traces of pitch and formants in (d) are extracted.

pitch harmonics become larger where they cross the formant traces.

V. Summary

The frequency-domain Prony method was proposed. It is an exact DFT-based method for AR model identification and sinusoidal parameter estimation. It is based on the AR model expressed by Fourier coefficients, and describes algebraic relations of sinusoid among Fourier coefficients. It uses Fourier coefficients as observables, which describe the overall changes in the waveform in the observation interval. Therefore, it performs well in noise and realizes higher statistical efficiency. Owing to the frequency decomposition capability of the method, it provides both single-tone estimators for isolated sinusoids and multi-tone or overall estimators for proximate or unresolvable sinusoids. In the frequency-decomposed procedures around selected peaks of Fourier coefficients distribution, the computation is low in cost and well conditioned. All of these will be important for applications to real-world signals with plural harmonics and their mixtures.

References

[1] R. Prony, "Essai experimental et analytique: sur les lois de la dilatabilite de fluides elastique et sur celles de la force expansive de la vapeur de l'alkool, a differentes temperatures," *J. de l'Ecole Polytechnique Floreal et Plairial, an III*, vol. 1, no. 22, pp. 24–35, 1795.

[2] M. L. Van Blaricum and R. Mittra, "A technique for extracting the pole and residues of a system directly from its transient response," *IEEE Trans. Antennas Propag.*, vol. 23, no. 6, pp. 777–781, Nov. 1975.

[3] D. W. Tufts and R. Kumaresan, "Frequency estimation of multiple sinusoids: Making linear prediction perform like maximum likelihood," *Proc. IEEE*, vol. 70, no. 9, pp. 975–989, Sep. 1982.

[4] R. Kumaresan, D. W. Tufts, and L. L. Scharf, "A Prony method for noisy data: Choosing the signal components and selecting the order in exponential signal models," *Proc. IEEE*, vol. 72, no. 2, pp. 230–233, Feb. 1984.

[5] S. M. Kay, "Accurate frequency estimation at low signal-to-noise ratio," *IEEE Trans. Acoust., Speech, Signal Process.*, vol. ASSP-32, no. 3, pp. 540–547, Jun. 1984.

[6] T-H. Li and B. Kedem, "Iterative filtering for multiple frequency estimation," *IEEE Trans. Signal Process.*, vol. 42, no. 5, pp. 1264–1268, May 1994.

[7] R. Roy, A. Paulraj, and T. Kailath, "ESPRIT–A subspace rotation approach to estimation of parameters of cisoids in noise," *IEEE Trans. Acoust. Speech, Signal Process.*, vol. ASSP-34, no. 5, pp. 1340–1342, Oct. 1986.

[8] P. Stoica and T. Söderström, "Statistical analysis of MUSIC and subspace rotation estimates of sinusoidal frequencies," *IEEE Trans. Signal Process.*, vol. 39, no. 8, pp. 1836–1847, Aug. 1991.

[9] J. Gillard, "Cadzow's basic algorithm, alternating projections and singular spectrum analysis," *Stats. Inter.*, vol. 3, pp. 335–343, 2010.

[10] B. N. Bhaskar, G. Tang, and B. Recht, "Atomic norm denoising with applications to line spectral estimation," *IEEE Trans. Signal Process.*, vol. 61, no. 23, pp. 5987–5999, Dec. 2013.

[11] B. G. Quinn, "Estimation of frequency, amplitude, and phase from the DFT of a time series," *IEEE Trans. Signal Process.*, vol. 45, no. 3, pp. 814–817, Mar. 1997.

[12] M. D. Macleod, "Fast nearly ML estimation of the parameters of real or complex single tones or resolved multiple tones," *IEEE Trans. Signal Process.*, vol. 46, no. 1, pp. 141–148, Jan. 1998.

[13] C. Candan, "A method for fine resolution frequency estimation from three DFT samples," *IEEE Signal Process. Lett.*, vol. 18, no. 6, pp. 351–354, Jun. 2011.

[14] P. Stoica, "List of references on spectral line analysis," *Signal Process.*, vol. 31, no. 3, pp. 329–340, 1993.

[15] S. M. Kay, *Fundametals of Statistical Signal Processing: Estimation Theory*, Englewood Cliffs, NJ, USA: Prentice Hall, 1993.

[16] B. G. Quinn and E. J. Hannan, *The estimation and tracking of frequency*, Cambridge, U.K.: Cambridge Univ. Press, 2001.

[17] A. Serbes, "Fast and efficient sinusoidal frequency estimation by using the DFT coefficients," *IEEE Trans. Commun.*, vol. 67, no. 3, pp. 2333–2342, Mar. 2019.

[18] Y. Xia, Y. He, K. Wang, W. Pei, Z. Blazic, and D. P. Mandic, "A complex least squares enhanced smart DFT technique for power system frequency estimation," *IEEE Trans. Power Del.*, vol. 32, no. 3, pp. 1270–1278, Jun. 2017.

[19] S. Scherr, S. Ayhan, B. Fischbach, A. Bhutani, M. Pauli, and T. Zwick, "An efficient frequency and phase estimation algorithm with CRB performance for FMCW radar applications," *IEEE Trans. Instrum. Meas.*, vol. 64, no. 7, pp. 1868–1875, Jul. 2015.

[20] T. Tyagi and P. Sumathi, "Frequency estimation techniques in capacitance-to-frequency conversion measurement," *Rev. Scientific Instrum.*, vol. 91, no. 1, 2020, Art. no. 015005.

[21] F. Engels, P. Heidenreich, A. M. Zoubir, F. K. Jondral, and M. Wintermantel, "Advances in automotive radar: A framework on computationally efficient high-resolution frequency estimation," *IEEE Signal Process. Mag.*, vol. 34, no. 2, pp. 36–46, Mar. 2017.

[22] S. Ando and T. Nara, "An exact direct method of sinusoidal parameter estimation derived from finite Fourier integral of differential equation," *IEEE Trans. Signal Process.*, vol. 57, no. 9, pp. 3317–3329, Sep. 2009.

[23] T. Nara and S. Ando, "Direct localization of poles of meromorphic function from measurements on incomplete boundary," *Inverse Problems*, vol. 26, 2010, Art. no. 015011.

[24] S. Ando, T. Nara, and T. Levy, "Partial differential equation-based localization of a monopole source from a circular array," *J. Acoust. Soc. America*, vol. 134, no. 4, pp. 2799–2813, 2013.

[25] S. Ando, T. Nara, and T. Kurihara, "Spatial filtering velocimetry revisited: Exact short-time detecting schemes from arbitrarily small-size reticles," *Meas. Sci. Technol.*, vol. 25, no. 8, 2014, Art. no. 085001.

[26] Y. Bresler and A. Macovski, "Exact maximum likelihiood parameter estimation of superimposed exponential signals in noise," *IEEE Trans. Acoust. Speech, Signal Process.*, vol. ASSP-34, no. 5, pp. 1081–1089, Oct. 1986.

[27] P. Stoica, P. Handel, and T. Söderström, "Approximate maximum likelihood frequency estimation," *Automatica*, vol. 30, no. 1, pp. 131–145, 1994.

[28] National Institute of Informatics, Speech Resources Consorcium, Japan, [Online]. Available: http://research.nii.ac.jp/src/en/index.html, dataset: AWA-LTR.

Shigeru Ando (Member, IEEE) received his B.E., M.E., and Dr. Eng. degrees in mathematical engineering and information physics from the University of Tokyo in 1974, 1976, and 1979, respectively. He joined the Faculty of Engineering of the University of Tokyo in 1979, and served as an Associate Professor from 1987. He also served as Professor from 1995 to 2016, and he is currently a Professor Emeritus at the Department of Mathematical Engineering and Information Physics, and the Department of Information Physics and Computing, the University of Tokyo. His interests are in image processing, signal processing, optical and acoustic sensing, and bio-inspired visual, auditory, and tactile sensor devices. He is a member of the Acoustical Society of America, the Optical Society of America, and the Society of Industrial and Applied Mathematics (SIAM).